

Research

Enhancing the durability and antibacterial activity of glass ionomer restorative material enriched by L-arginine and nano-titanium for pit and fissure sealing

Hanaa Mahmoud Elgamily¹  · Emad Aboalazm² · Engie M. Safwat¹ · Ahmed M. Youssef³

Received: 7 October 2023 / Accepted: 1 January 2024

Published online: 26 January 2024

© The Author(s) 2024 [OPEN](#)

Abstract

Background Sealing teeth' pits and fissures is of prime importance in preventing caries. Despite the evidenced bioactivity of glass-ionomer cements (GICs), they still fail to totally inhibit caries. This partially might be due to their insufficient antibacterial and strength properties. L-arginine (Arg) has superior caries-preventive potential thanks to its prebiotic-based biofilm-modulating effect. Titanium dioxide (TiO₂) on the other hand, has well-known antibacterial characteristics, and being in nano size is supposed to improve strength. Therefore, this study aims to improve the antibacterial efficiency and the mechanical properties of conventional GICs using 1% Arg and 3% TiO₂ nanoparticles for pit and fissure sealing.

Methods Etched enamel surfaces of 100 extracted human third molars were randomly divided into two groups; a control group, where teeth were restored using glass ionomer Ionofil Plus, and an experiment group, where teeth were restored using glass ionomer Ionofil Plus incorporating Arg–TiO₂. Specimens of both groups were tested for microleakage, enamel shear bond strength, and fluoride ion release using a stereo microscope, universal testing machine, and ion chromatography ICs 5000+ SP respectively. Surface analysis was conducted through scanning electron microscopy coupled with energy-dispersive X-ray analysis (SEM–EDX) and atomic force microscope (AFM). Furthermore, specimens of both groups were incubated with *Streptococcus mutans*, *Lactocaseibacillus rhamnosus*, and *Actinomyces viscosus* for quantitative antibacterial evaluation, compared to a specimen-free control using adherent/planktonic bacterial count test.

Results The experimental group had statistically lower microleakage percentage, higher shear bond strength, and constant fluoride release compared to the control group at $P=0.01$, 0.002 , and <0.001 respectively. SEM of the experimental group revealed hybrid particles of the Arg–TiO₂ incorporating GIC with clusters of uniformly distributed TiO₂ nanoparticles. AFM showed lower surface roughness for the experimental group indicating its homogeneity. The adherent probiotic *L. rhamnosus* bacterial count had the highest count in Arg–TiO₂ (IP) GIC group ($P < 0.001$) with lack of adherent pathogenic *S. mutans* bacterial count compared to planktonic/adherent *S. mutans* bacterial count in the control group and (IP) GIC group ($P < 0.05$).

Conclusions Incorporating 3% TiO₂ nanoparticles and 1% Arg in GICs can enhance their mechanical properties, fluoride release, and antimicrobial efficiency.

Keywords Glass-ionomer cements · TiO₂ nanoparticles · L-arginine · Pit and fissure sealants · Microleakage · Antibacterial activity

✉ Hanaa Mahmoud Elgamily, hm.elgamily@nrc.sci.eg | ¹ Restorative and Dental Materials Department, Oral and Dental Research Institute, National Research Centre, 33 El Bohouth Street (Former El Tahrir Street), Dokki, P.O. 12622, Giza, Egypt. ² Department of Restorative Dentistry, Faculty of Dentistry, Egyptian Russian University, Badr, Cairo, Egypt. ³ Packaging Materials Department, Chemical Industrial Institute, National Research Centre, Giza, Egypt.



1 Background

Dental pit and fissure sealing is considered an efficient, non-invasive method of avoiding caries in children and adolescents. Patients with multiple caries, deep, narrow pits and fissures in molars and premolars are at high caries risk and are suggested to get sealants [1–5].

Glass-ionomer cements (GICs) are commonly used in clinical dentistry for several applications, including fissure sealants, luting agents, complete restorations, liners and bases [6]. Their biocompatibility [7], fluoride-releasing capability [8, 9], and adhesion to the tooth surface [10, 11], make them typically desirable for such applications.

Secondary caries continues to be the main reason for the GIC restorations' failure despite enclosing bioactive fluoride (F) that helps restrict demineralization and boost remineralization [12]. This can be linked to the fact that F is ineffective in controlling biofilm formation [13]. Bacterial biofilm at the edges of GIC restorations can initiate microleakage with subsequent secondary caries [14, 15]. Given the material's wide range of clinical applications, the treatment plan involving GICs must therefore be enhanced, either by adding a biofilm inhibitory agent or a biofilm modifying drug, thus stopping the development of biofilm-mediated caries [16]. Altering the biofilm ecology next to a restoration from pathogenesis to equilibrium prevents the microbiome dysbiosis attributed to caries developing [17].

Arginine (Arg), being a semi-essential amino acid, is known as a prebiotic-based biofilm modulator. Its inclusion in fluoride toothpaste formulations proved to have superior caries-preventive impact when compared to the matched controls (containing F) [18, 19]. Arg is metabolized by *Streptococcus sanguinis*, *Streptococcus parasanguinis*, and *Streptococcus gordonii* creating ammonia that balances the acidic pH in the oral cavity [20, 21]. It has been shown that fluoride inhibits *Streptococcus mutans* growth while boosting *S. sanguinis* development [22]. Arg inhibits the pathogenic biofilm matrix formation and restores the pH balance of the biofilm to normal. By preserving healthy oral biofilms, the oral microbial ecology is influenced [23–26]. Hence, adding Arg to GICs helps improve the chance of biofilm homeostasis and prevents the development of secondary caries at the tooth-GICs' interface.

In general, the mechanical properties of GICs are improved by the addition of filler particles, yet fillers can negatively impede the cement's antibacterial effect and disrupt their bacterial metabolism [27]. The size of filler particles likewise plays a crucial role in affecting both mechanical and antibacterial properties. The studies of using nanoparticles (NPs) in dentistry have substantially expanded, with a particular focus on improving mechanical characteristics and antibacterial effects. One of the published researches revealed that the mechanical characteristics and bond strength of conventional GICs were enhanced by the addition of hydroxyapatite and fluorapatite nano bioceramics [28]. Another study focused on using titanium dioxide (TiO₂) powder due to its chemical stability, biocompatibility, and antibacterial characteristics, thus holds great potential as an inorganic filler [29].

It appears promising to incorporate Arg as a biofilm modifier and TiO₂ nanopowder as an antibacterial and reinforcing agent, at ideal concentrations according to previous literature [16, 29–31], without impairing the physical, chemical, and mechanical properties of GICs, thus provides GICs with the clear caries-preventive effect of the biofilm modifiers and the antibacterial and reinforcement significant use of nanoparticles. As far as the authors know, no previous literature studied the effect of adding both Arg and TiO₂ nano-particles to GICs. Consequently, this study aims to investigate the microleakage, enamel micro shear bond strength, surface topography, fluoride release, and bacterial adhesion of conventional glass ionomer cement supplemented with Arg and TiO₂ nano-particles for use as pit and fissure sealant. The null hypothesis tested was that there was no efficacy when incorporating Arg–TiO₂ into GIC on its mechanical and antibacterial potential.

2 Methods

2.1 Ethics approval

All performed procedures were carried out in accordance with relevant ethical guidelines and regulations of the Helsinki Declaration. The Medical Research Ethics Committee (MREC), National Research Centre of Egypt, approved all experimental protocols under reference number "24402/2023". For the collection of isolated teeth and saliva collection from a single donor, informed consents were obtained from all participants.

2.2 Formulation of the experimental Arg–TiO₂ (IP) GIC group

Titanium dioxide nanoparticles with anatase phase and particle size < 25 nm (Sigma-Aldrich, St. Louis, MO, USA) were combined with the powder of (IP) GIC at 3% (w/w) in a vortexor (Vortex-2Genie, Scientific Industries, Bohemia, USA) for 1 min [30]. L-arginine powder (A-5006, Sigma Aldrich, St. Louis, USA) was then added at a concentration of 1% (w/w) to the previous mixture, the whole mixture was thoroughly vortexed for 2 min and then kept in a sterile tube (Bijou, Thermo Scientific, Newport, UK) [16]. GIC (GC Corporation) was kept at the manufacturer's recommended powder-to-liquid ratio of 2.7/1.0 g.

Characterization of TiO₂ nano particles was done using X ray diffraction (XRD) via a Philips X-ray diffractometer (PW1930 generator, PW 1820 goniometer) through radiation of Cu K α source (45 kV, 40 mA, with $\lambda = 0.15418$ nm) using 2 θ range of 5°–80° concluded the size of a step of 0.02 as well as a 1 s time for each step. Transmission electron microscopic images (TEM, Model: JEOL-JEM-1400) were correspondingly obtained for TiO₂ nano-particles where one drop of TiO₂ solution was placed on a copper grid for investigation.

2.3 Processing of the specimens

A total of 100 freshly extracted impacted human third molars were collected with informed consent and kept in saline solution at 4 °C for up to 1 month. Using open-source software (GPower, Germany, <http://www.gpower.hhu.de>) [32], the sample size was computed. The power for the study was 0.80, with an effect size of 0.6 and α error of 0.07 for 10 teeth in each test of the group. Teeth' pits and fissures were cleaned using a low-speed, water-cooled revolving brush after surface debridement with a hand-scaling tool, then teeth were pre-treated by etching (Super-Etch TM 37% phosphoric acid etch, SDITM, Bayswater, Victoria, Australia) for 30 s, followed by 10 s washing and 5 s drying using a triple syringe. After that, the sealant was homogenously applied to the etched enamel. According to the type of the pit and fissure sealant applied, teeth were randomly assigned into two main groups (n = 50); the control (IP) GIC group, where glass ionomer Ionofil Plus (IP) (VOCO, GmbH, Cuxhaven, Germany) was applied, and the experimental Arg–TiO₂ (IP) GIC group, where glass ionomer Ionofil Plus (IP) incorporating Arg–TiO₂ was applied.

2.4 Microleakage assessment

Ten specimens from each group (n = 10) were put through 1000 thermo-cycles in water baths ranging in temperature from 5 to 55 °C (30 s for each bath, 5 s between baths), using a thermocycler THE-1100 (SD Mechatronik GmbH, Feldkirchen-Westerham, Germany). The specimens were thermocycled and then stored in a water bath at 37 °C for 1 week. The apices of the teeth were thereafter covered with self-curing methyl methacrylate resin (UNIFAST Trad, GC, America Inc. Alsip, IL, USA), and all surfaces were painted with nail polish except for 2 mm along the edges of the fissures [33].

All teeth specimens were immersed in a 1% methylene blue solution (Merck14279, Darmstadt, Germany) for 24 h at 22 °C to allow the dye to reach any potential gaps between the dental materials and the sealant. After being rinsed, the specimens were divided longitudinally into two to three parts per tooth using a water-cooled electric diamond saw (Microslice 2TM; Ultratec, Santa Ana, CA, USA). After being divided into smaller pieces, the slides were inspected under a stereo microscope (NIKON SMZ25, 25X, Germany), taken with a digital camera (FinePix, Fujifilm Co., Tokyo, Japan), and the photos were then downloaded to a PC (personal computer) to be evaluated for microleakage and penetration. Using computer measurements of the photographic representation of the dye penetration, the percentage of dye penetration over the whole length of the sealant was calculated. By dividing the length of the microleakage by the length of the tooth-sealant interface using image analysis software (Sigmascan®, SPSS; Jandel Scientific, San Rafael, CA, USA) calibrated to a millimeter ruler, the microleakage proportion was quantitatively analysed [34].

2.5 Enamel shear bond strength evaluation

Each tooth specimen in both groups (n = 10) was separately fixed in acrylic resin (NicTone 62, MDC Dental, Guadalajara, Mexico), and the labial surface of each tooth was aligned using a mounting jig. Meanwhile, standardized blocks of both the control (IP) GIC group and the experimental Arg–TiO₂ (IP) GIC group were prepared using a rectangular metal mold (4 × 4 × 1 mm). Prior to cementing the block to the tooth, teeth surfaces were polished with #400 waterproof abrasive paper (Fuji Star, Sankyo, Rikagaku, Okegawa, Japan) then the vestibular surfaces were sandblasted for 1 min with 50 μ m of aluminum dioxide (Micro Cab, Danville, San Ramon, CA, USA). After that, teeth received 1 min of ultrasonic cleaning

(Quantrex, Kearny, NJ, USA) [16]. A universal testing device (Instron 3345, Instron Corporation, England) with a 1-kN (kilo newton) load cell and a crosshead speed of 1 mm/min was used to measure the shear bond strength of both groups to enamel. Force was applied at the block-dental surface interface. The ultimate shear load to failure was recorded in Newton (N). By dividing the highest ultimate load to failure (N) by the bonded cross-sectional area (mm^2) through machine software analysis (BlueHill 3, Instron, England), the average bond strength in MPa was calculated. Means and standard deviations were recorded [35–37].

2.6 Surface analysis using scanning electronic microscopy coupled with energy-dispersive spectroscopy (SEM–EDX) and atomic force microscopy (AFM).

Ten specimens from each group were desiccated in a Sanpla Dry Keeper (Sanplatec Co., Tokyo, Japan) for 48 h for SEM analysis examination. All specimens were examined under a SEM model Quanta 250 Field Emission Gun (FEI Company, Netherlands) with an accelerating voltage of 20 kV, and at a magnification of 600 \times and 1000 \times . EDX was performed on the identical SEM-measured specimens using a Kevex 8000 system (Kevex Corp., Foster City, California) at a 15 keV accelerating voltage, a magnification of 1000 \times , and an acquisition duration of 100 s. Five points per sample (300 mm^2 each) were randomly chosen for the EDX point analysis (80 mm^2 , SDD [silicon drift detector]) to determine Ca, P, C, Mg, and O ions in specimens. Relative weight percentages were calculated with a standardless semiquantitative analysis routine.

The surface topography of the same ten specimens of each group was analysed by Atomic force microscopy (Tosca 200 AFM—Anton Paar GmbH—Germany). Digital images were performed for each specimen at a data scale of 40 μm with resolution 400, using tapping mode and recorded with a slow scan rate (1 line/s at angle 0). Using the Tosca analysis program, the AFM data was processed following ISO 25178 [38].

2.7 Measuring fluoride ions release

Ten sealant specimens of both the control and the experimental group were prepared using a cylindrical split Teflon mold of 5 mm diameter and 1 mm thickness. Then they were put in 10 ml of pH-7.0 deionized water, and maintained at 37 °C. For measurements at 2, 6, 12, 24, and 72 h, the samples were transferred to fresh vials with new deionized water. To perform all analyses of fluoride concentration in a single session, the old deionized water was stored alongside the switch to new vials at – 20 °C. The samples were filtered using Merman filter paper before being analyzed on an Ion Chromatography ICs 5000+ SP (Thermo Scientific, USA) system that includes an automated sample injector and a P680 pump. A personal computer running Dionex Chromeleon software was used for data collection and processing. The unit of measurement is mg/L or ppm. The water pollution research department (National Research Centre, Egypt) performed the analyses of the samples [39].

2.8 Quantitative evaluation of bacterial adhesion to the control and the experimental GIC Surfaces

2.8.1 Saliva collection

After chewing on a rubber band, a single donor's whole saliva (WS) was extracted through expectoration and placed in ice-chilled tubes. Centrifugation was used to clarify the WS (17,000g, 30 min). The clarified WS was then used in the anti-adherence study [40].

2.8.2 Bacterial strains and growth conditions

Streptococcus mutans (ATCC 25175), *Lactobacillus rhamnosus* (NRRL B-442), and *actinomyces viscosus* (ATCC 19246) were obtained from MIRCEN (Microbiological Resources Centre, Cairo, Egypt). Bacterial cells of each strain were grown in Tryptic Soy Broth (TSB; Merck KGaA 64271 Darmstadt, Germany), and the concentration was adjusted to 107 CFU/ml using the McFarland spectrophotometric method at OD600nm (Spectrophotometer, DU 730 Life Science, Beckman Coulter, California, USA) [16, 39]. The inner surfaces of 75 \times 12 mm borosilicate glass culture tubes were treated for 2 min with 2 ml cleared saliva to create saliva-coated glass culture tubes. After that, sterile distilled water was used to quickly rinse the surface. Each saliva-coated culture tube received 2 ml bacterial solution along with a multi-species inoculum prepared in a ratio of 1:1:1:1 then incubated for 18–20 h at 37 °C [41]. Both the control and the experimental sealant were prepared into cylindrical molds (10 mm in diameter and 2 mm in thickness). Ten discs of each group were dipped

separately into the previously treated saliva-coated culture tubes. Then, 2 ml of Tryptic Soy Broth media (TSB; Merck KGaA 64271 Darmstadt, Germany) supplemented with 5% (w/v) sucrose was added and one saliva-coated culture tube containing bacterial suspension and TSB medium was left as a control without specimen. All testing tubes were incubated for 72 h in an anaerobic chamber (85% N₂, 10% H₂, 5% CO₂, 37 °C), while positioned at a 300 angle from the horizontal to increase the surface area for bacterial adherence [39].

2.8.3 Adherent/planktonic bacterial count test

Specimens from each group with adherent bacteria were removed using 0.5 M NaOH, centrifuged, and suspended in saline [42]. Each suspension, containing adherent and non-adherent bacteria from each group, separately underwent a 1-min sonication cycle after 2 min of vortexing. Then, saline dilutions of 1×10^{-2} and 1×10^{-3} were carried out with a suspension that had previously been vortexed and sonicated [43]. Thirty μ l of each dilution was spread on the surface of selective media Mitis Salivarius Bacitracin (MSB; BD Difco, France) plate for *S. mutans*, MRS medium (Merck, Darmstadt, Germany) for *L. rhamnosus*, and Blood Agar Base No.2 with Horse Blood (Thermo Scientific™ PB0114A, UK) for *A. viscosus*. The suspensions containing adherent or non-adherent (planktonic) bacteria were counted to measure the number of colony-forming units per ml (CFU/ml) at both dilutions of 10^{-2} and 10^{-3} after an anaerobically incubation period of 48 h at 37 °C.

2.9 Statistical analysis

Data was checked for normality using Kolmogorov–Smirnov and Shapiro–Wilk tests. Microleakage percentage and proportion, Shear bond strength, and Fluoride release data showed normal distribution, independent t-test was used to compare between tested groups. For bacterial count, data showed a non-normal distribution, Kruskal–Wallis test was used to compare different types of bacteria. The significance level was set at $P=0.05$ (SPSS IBM, version 23, Armonk, NY, USA).

3 Results

3.1 Results of TiO₂ characterization via X-ray diffraction pattern and TEM image examination

The structure of TiO₂ nanoparticles was assessed using X-ray diffraction pattern, the five main peaks are detected in the XRD pattern of TiO₂ nanoparticles (Fig. 1a) at 24.97°, 39.36°, 47.59°, 54.94° and 62.18° for 2 theta angles between 5° and 80°, these peaks can be attributed to various diffraction planes of anatase TiO₂. Furthermore, the four separate peak patterns are seen at 24.97°, 37.36°, 53.44°, and 69.32°, which can be attributed to various rutile phases of TiO₂ diffraction planes. The TiO₂ nanoparticles XRD examination showed that 25% of the nanoparticles are rutile and 75% are anatase. The morphology of nanoparticles was evaluated using TEM. The TEM observation was performed for TiO₂ nanoparticles as shown in (Fig. 1b). It shows that TiO₂ particles are in the range of nanometer scale and have good dispersive ability,

Fig. 1 TiO₂ characterization results showing; XRD of TiO₂ nanoparticles (A) and TEM image of TiO₂ nanoparticles (B)

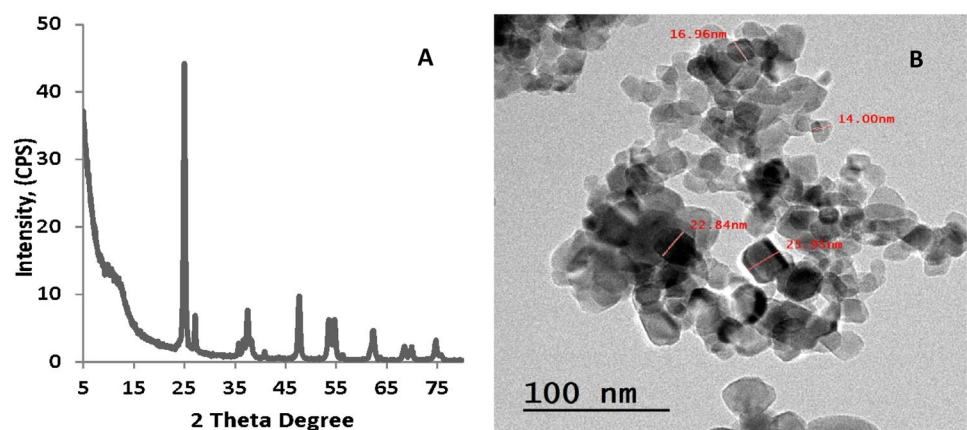
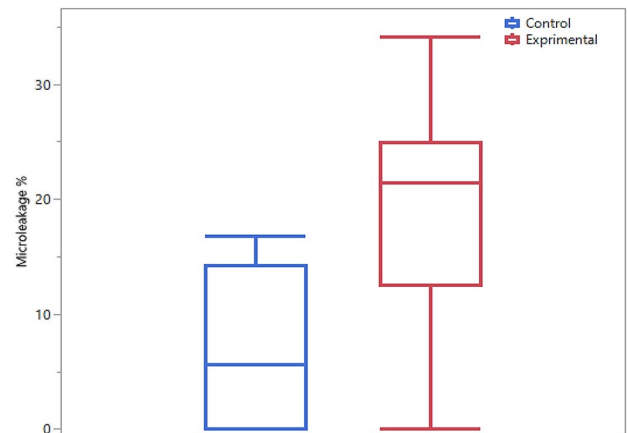


Table 1 Descriptive statistics for microleakage percentage between study groups

	Experimental Arg-TiO ₂ (IP) GIC group	Control (IP) GIC group
Number of samples	10	10
Mean microleakage	6.90	18.80
Standard deviation	7.02	10.94
Median	5.59	21.41
Minimum	0.00	0.00
Maximum	16.81	34.14

Fig. 2 Box plot describing the microleakage percentage data of both groups

which should have a positive effect on their biological properties. The TiO₂ nanoparticles revealed a regular shape with a particle size range of 14–25 nm.

3.2 Microleakage and penetration results

Table 1 and Fig. 2 represent the total length percentage of the sealant that the dye penetrated. Results of both groups showed dye microleakage beneath the sealants, however the experimental Arg-TiO₂ (IP) GIC group had a significantly less microleakage % [mean: 6.90 ± 7.02 (SD)] compared to the (IP) GIC group [mean: 18.80 ± 10.94 (SD)] at $P=0.01$. Regarding microleakage proportions, the microscope depiction in Fig. 3 demonstrated that the (IP) GIC group [mean: 0.19 ± 0.11 (SD)] had a higher dye penetration ability than the experimental Arg-TiO₂ (IP) GIC group [mean: 0.07 ± 0.07 (SD)] at P value=0.01.

3.3 Enamel shear bond strength results

As demonstrated in Table 2, the experimental Arg-TiO₂ (IP) GIC group recorded higher statistically significant values whether in the maximum shear load to failure [mean 64.14 ± 10.33 (SD)] or the mean shear bond strength [mean 9.18 ± 1.51 (SD)] than those for the control (IP) GIC group [mean 47.55 ± 9.93 (SD)] and [mean 6.73 ± 1.40 (SD)] respectively at $P=0.002$.

3.4 Results of surface analysis using SEM-EDX and AFM

SEM micrographs (600× and 1000×) of the control (IP) GIC specimens are shown in Fig. 4A1 and A2, particles appeared to be adequately dispersed and microcracks on the surface were evidenced. At the higher magnification in Fig. 4A3, an extensive gap of approximately 32.8 ± 2 μm in width was present throughout the glass ionomer Ionofil Plus (IP) and enamel inter surfaces.

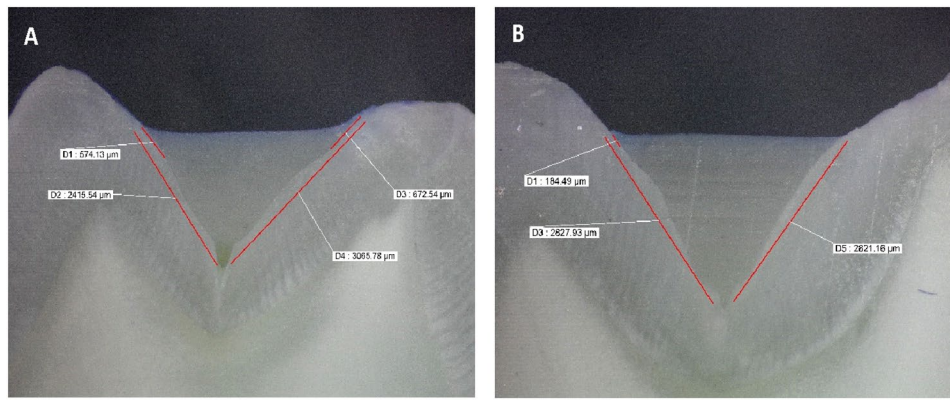


Fig. 3 Representative depiction for illustrating the method used to measure the microleakage proportion (penetration ability) for the control (IP) GIC group **(A)** and the experimental Arg-TiO₂ (IP) GIC group **(B)**. D₁ and D₃ in this figure **(A)** and D₁ in **(B)** represent the length of microleakage in μm. D₂ and D₄ in **(A)** and D₃ and D₅ in **(B)** represent the length of the sealant in μm. The proportion of microleakage in **(A)** for the control (IP) GIC group = $D_1 + D_3 / D_2 + D_4$, while that for the experimental Arg-TiO₂ (IP) GIC group in **(B)** = D_1 / D_3

Table 2 Descriptive statistics for the maximum load and shear bond strength data between study groups

	Experimental Arg-TiO ₂ (IP) GIC group					Control (IP) GIC group					P value
	Mean	SD	Median	Min	Max	Mean	SD	Median	Min	Max	
Max load	64.14	10.33	65.26	48.75	77.63	47.55	9.93	46.57	32.30	63.80	0.002
Shear bond	9.18	1.51	9.59	6.90	10.98	6.73	1.40	6.59	4.57	9.03	0.002

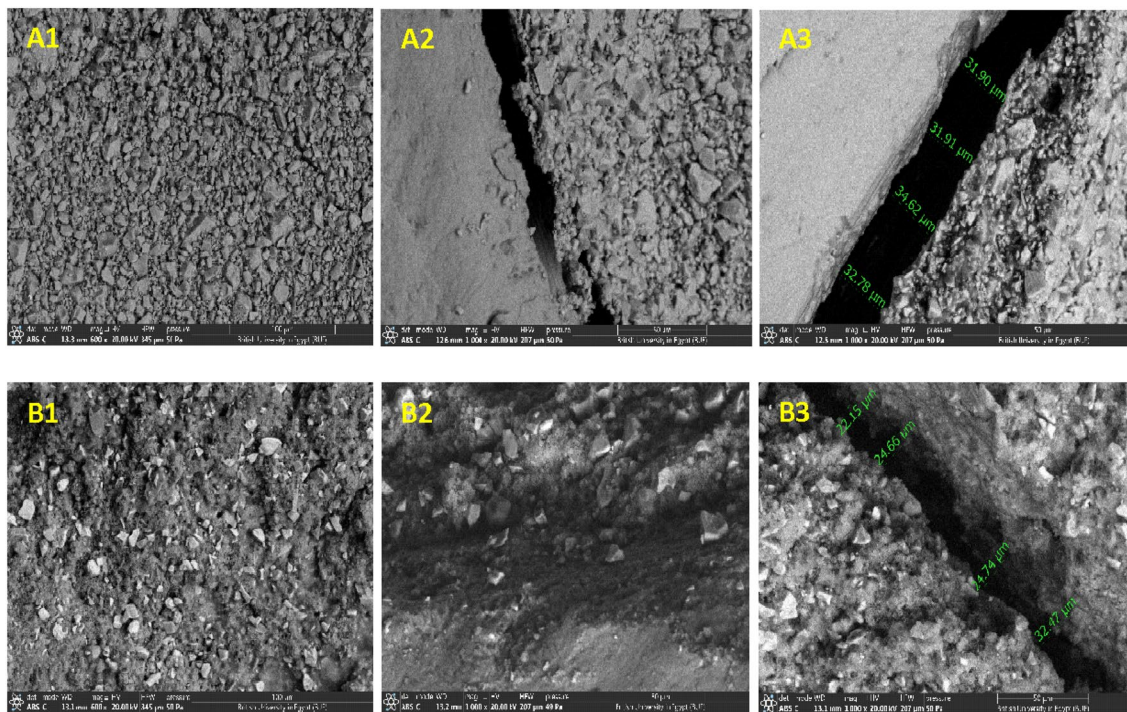


Fig. 4 Represents scanning electron micrograph of the control (IP) GIC sealant **(A)** and the experimental Arg-TiO₂ (IP) GIC **(B)**, where **A1** is the image at original magnification (600×) showing adequately dispersed particles, **A2** and **A3** are higher magnification images (1000×) revealing microcracks at the inter surface between (IP) GIC and enamel with an approximately $32.8 \pm 2 \mu\text{m}$ width. **B1** is the original magnification image (600×) showing hybrid particles of the Arg-TiO₂. **B2** and **B3** are higher magnification images (1000×) revealing the unreacted TiO₂ particles within the matrix a gap was found within the Arg-TiO₂ (IP) GIC sealant with $\approx 24 \mu\text{m}$ width

SEM observations of the experimental Arg-TiO₂ (IP) GIC specimens (Fig. 4B1 and B2) revealed hybrid particles of the Arg-TiO₂ incorporating glass ionomer Ionofil Plus. Due to their angular and semispherical shapes, some deposited microparticles, appear to be clusters of TiO₂ nanoparticles that are uniformly positioned between (matrix) macroparticles. Nevertheless, a microcrack within the salt matrix of approximately 24 μm width was revealed (Fig. 4B3).

EDX results from different locations for both the control (IP) GIC and the experimental Arg-TiO₂ (IP) GIC group as shown in Fig. 5A and B respectively. We should note that strontium which is present in the control (IP) GIC is not detected in experimental Arg-TiO₂ (IP) GIC. However, the experimental Arg-TiO₂ (IP) GIC revealed to have comparatively substantial levels of titanium (added as titanium dioxide). On both surface sealants, smaller levels of silicon, aluminium, and minor amounts of salt and phosphorus were found. EDX also showed lighter elements like fluorine

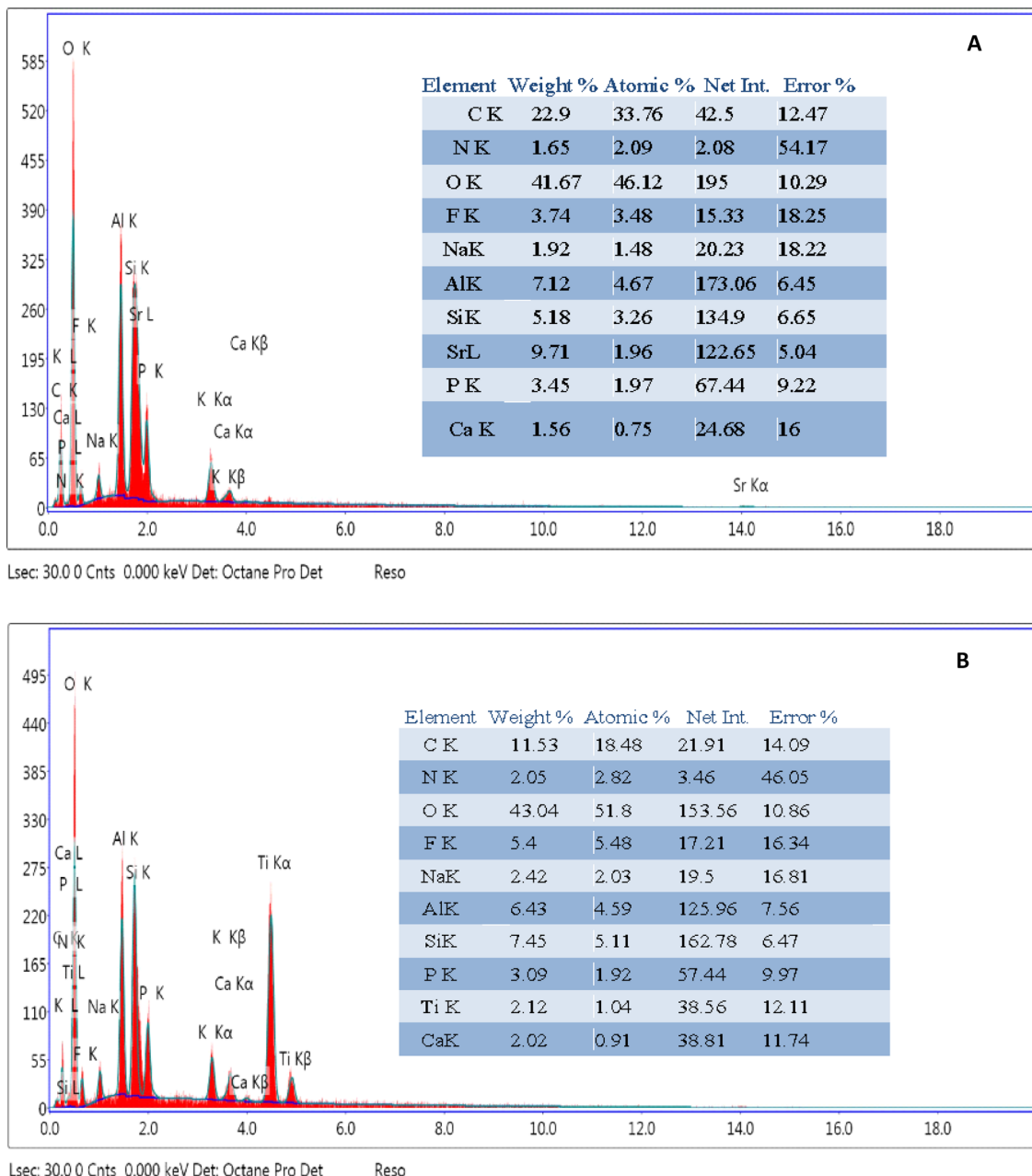


Fig. 5 EDX analysis represented by the weight percentages of chemical elements and the graphic representation of the net peak intensities collected on the control (IP) GIC (**A**) and experimental Arg-TiO₂ (IP) GIC (**B**) specimen surfaces. The X-ray spectra were collected with an accelerating voltage of 20 kV

Fig. 6 Three-dimensional AFM images representing; the control (IP) GIC group (**A**) where peaks and valleys were observed, producing undulations in surface texture, and the experimental Arg-TiO₂ (IP) GIC group (**B**) where the surface was flatter with less observed peaks and valleys

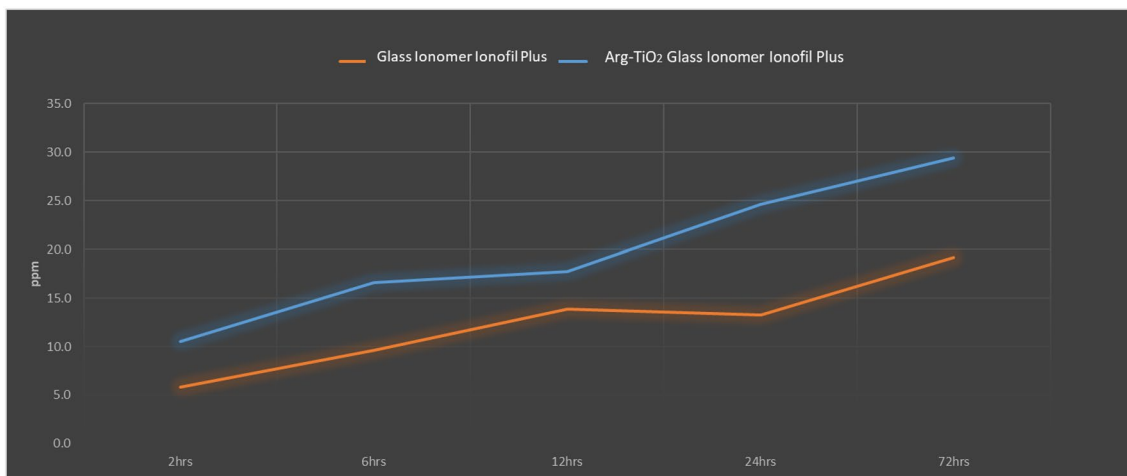
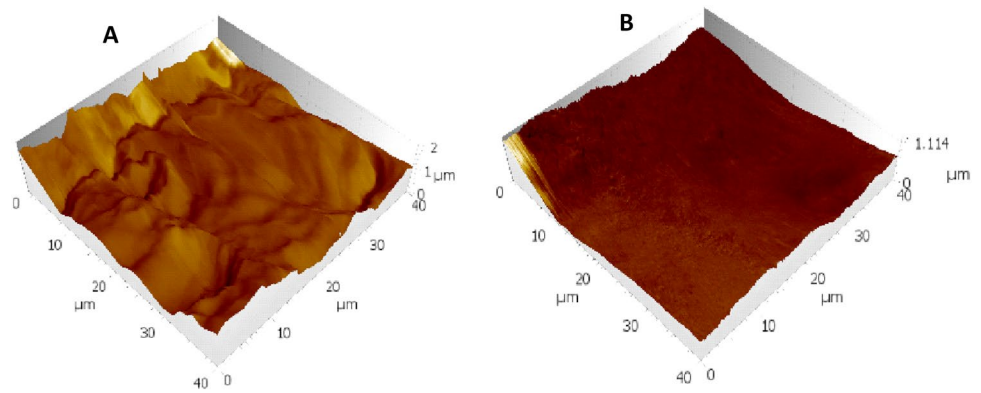


Fig. 7 Line chart representing fluoride release (ppm/mg) from baseline to 72 h for the two-sealant groups

and carbon. The element with the highest weight percentage in the Arg-TiO₂ (IP) GIC group compared to the (IP) GIC group was fluorine.

As regards the AFM analysis presented in Fig. 6, changes in surface topography and surface texturing occurred when Arg-TiO₂ was introduced to the (IP) GIC. These modifications include matrix adjustments and the insertion of hybrid particles. In Fig. 6A, the control (IP) GIC specimens, peaks and valleys were observed, producing undulations in surface texture where the maximum peak height (*S_p*) and Maximum pit height (*S_v*) were 1.235 μm and 0.8586 μm respectively. On the contrary, the surface quality of the experimental Arg-TiO₂ (IP) GIC specimens became flatter than the control (IP) GIC group as seen in Fig. 6B, where (*S_p*) was 0.7227 μm and (*S_v*) was 0.3914 μm. The sums of the largest peak height value and the largest pit depth value in the defined area (*S_z*) were 2.093 μm and 1.114 μm for the control (IP) GIC and the experimental Arg-TiO₂ (IP) GIC respectively. In addition, the average surface roughness (*S_a*) value was 0.1897 μm in the control (IP) GIC and 1.260 μm in the experimental Arg-TiO₂ (IP) GIC. According to these results, the surface roughness of the control (IP) GIC is greater than that of the experimental Arg-TiO₂ (IP) GIC.

3.5 Measurements of fluoride ions release

For both the control (IP) GIC and the experimental Arg-TiO₂ (IP) GIC groups, the mean fluoride release increased from baseline till 12 h. After 12 h, the fluoride release was different between both sealants ($P < 0.001$). The GIC group for Arg-TiO₂ (IP) GIC demonstrated the greatest fluoride release mean value at 24 and 72 h. In contrast, the mean fluoride release for the (IP) GIC group declined after 12 h until 24 h, then increased once again after reaching 72 h. Throughout the test periods, all test specimens emitted detectable levels of fluoride (Fig. 7).

Table 3 Descriptive statistics Log₁₀ CFU/ml between different tested bacteria for all groups

(10 ⁻²) Log ₁₀ CFU/ml	<i>S. mutans</i>					<i>L. rhamnosus</i>					<i>A. viscosus</i>					P value
	Mean	SD	Median	Min	Max	Mean	SD	Median	Min	Max	Mean	SD	Median	Min	Max	
<i>Planktonic bacteria</i>																
Control	25.2 ^a	4.8	26.5	20.0	32.0	16.2 ^b	1.5	16.0	14.0	18.0	23.6 ^a	1.6	23.5	22.0	26.0	<0.001
(IP) GIC	14.4 ^b	0.7	14.5	13.0	15.0	17.1 ^a	1.0	17.0	15.0	18.0	6.3 ^c	1.3	6.0	5.0	9.0	<0.001
Arg-TiO ₂ (IP) GIC	6.7 ^a	2.6	7.0	4.0	10.0	3.3 ^b	0.9	3.0	2.0	5.0	6.8 ^a	1.7	6.5	5.0	10.0	<0.001
<i>Adherent bacteria</i>																
Control	24.4 ^a	2.1	25.0	20.0	26.0	3.6 ^c	2.3	3.0	1.0	7.0	6.6 ^b	1.2	6.5	5.0	8.0	<0.001
(IP) GIC	16.9 ^a	2.6	16.5	13.0	20.0	6.2 ^b	0.8	6.0	5.0	7.0	16.4 ^a	1.3	16.0	15.0	18.0	<0.001
Arg-TiO ₂ (IP) GIC	12.7 ^c	1.6	13.0	11.0	15.0	25.9 ^a	1.2	26.0	24.0	28.0	21.1 ^b	1.1	21.0	20.0	23.0	<0.001

Superscripts with Different small letters within mean row indicate significant difference at $p < 0.05$ (Dunn Bonferroni correction)

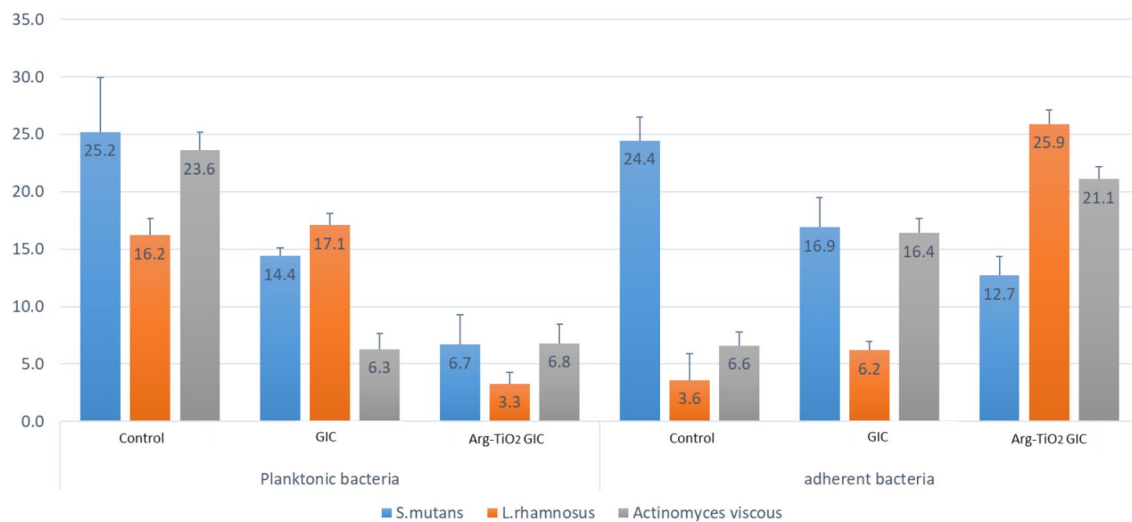


Fig. 8 A bar graph showing the averages of the planktonic and adherent bacterial counts (CFU/ml) for each tested group

3.6 Quantitative evaluation of antibacterial activity

Table 3 and Fig. 8 illustrate the means values of the adherent and planktonic bacterial counts (CFU/ml) for each group based on the bacterial counts of *S. mutans*, *L. rhamnosus*, and *A. viscosus*. Different tested bacteria showed a significant difference between each other for all groups at $P < 0.001$. Regarding the adherent bacteria in the experimental Arg-TiO₂ (IP) GIC group, a mean CFU/ml value of adherent *L. rhamnosus* bacterial count [25.9 ± 1.2] showed the highest statistically significant bacterial count, followed by the adherent *A. viscosus* [21.1 ± 1.1] and the lowest mean count was found in *S. mutans* [12.7 ± 1.6] at $P < 0.001$. Moreover, the mean CFU/ml value of adherent *L. rhamnosus* bacterial count for the experimental Arg-TiO₂ (IP) GIC group showed a statistically higher mean value compared to other adherent *L. rhamnosus* bacterial count in the control group [3.6 ± 2.3] and (IP) GIC group [6.2 ± 0.8] at $P < 0.05$. In the experimental Arg-TiO₂ (IP) GIC group lack of CFU/ml of adherent *S. mutans* bacterial count [12.7 ± 1.6] was noticed compared to planktonic/adherent *S. mutans* bacterial count in control group [25.2 ± 4.8/24.4 ± 2.1] and (IP) GIC group [14.4 ± 0.7/16.9 ± 2.6] at $P < 0.05$. For the adherent *A. viscosus* bacterial count, the highest bacterial mean value was found in (IP) GIC group (21.1 ± 1.1), followed by Arg-TiO₂ (IP) GIC group (16.4 ± 1.3), and the lowest mean value was in the control group (6.6 ± 1.2) at $P < 0.05$.

4 Discussion

Many studies are currently focusing on improving pit and fissure sealants in order to enhance their physical, mechanical and biological properties. In the present study, GIC pit and fissure sealant was modified by adding 3% Nanotitanium and 1% L-arginine, these specific percentages were selected in accordance with previous literatures [16, 29–31], where in a study conducted by Contreras et al. [30], 3% and 5% (w/w) TiO_2 nanoparticles were added to GIC and revealed no differences regarding mechanical and shear bond properties. However, our study selected the minimum concentration (3%), as high concentration could have a negative effect on bacterial viability contributed to microbiome dysbiosis of the GIC adherent biofilm, while minimum concentration could affect the virulence factors of bacteria (decrease bacterial count) but keep microbiome in balance.

Regarding L-arginine concentration, previous studies [34, 35], showed reduced surface roughness of GIC with lower concentrations of (1–2%) Arg. This was explained by the interaction between the positively charged guanidinium group of Arg and the electronegative F ion, created an Arg-encapsulated calcium-fluoro-alumino-silicate complex [16]. Thus authors built on these proved effective concentrations when inspecting the influence of adding both ingredients in the same sealant restoration, as none of the previous researches combined both ingredients in the same sealant.

Pits and fissures of the occlusal surface of the teeth are thought to be particularly susceptible to the adherence of cariogenic bacteria, which leads to the development of caries, thus their sealing is mandatory. However, microleakage is the main cause of sealant failure [44]. Dental sealants must adhere tightly to the enamel surface in order to prevent microleakage at the tooth-material contact with subsequent treatment failure [44]. The relative efficacy of various sealants still has to be determined. Restorative materials are developing more quickly than ever, and procedures are being used to assess how well each new material will fit a tooth without microleakage. From these procedures is the subjecting of the specimens to thermocycling, this in vitro procedure inspects microleakage at various temperatures mimicking what the teeth experience during eating and drinking under clinical circumstances [45]. In the current investigation, two dental fissure sealants were used to compare and detect microleakage, in conventional glass ionomer cement ((IP) GIC) and GIC supplemented with L-arginine (Arg), and titanium dioxide (TiO_2) nanopowder (Arg- TiO_2 (IP) GIC) bonded to enamel surface. The null hypothesis proposed that adding Arg- TiO_2 to GIC would not significantly alter microleakage when compared to (IP) GIC. The results showed that the experimental Arg- TiO_2 (IP) GIC group had a significantly less microleakage percentage than the (IP) GIC group. This could be attributable to the presence of titanium dioxide (TiO_2) nanoparticles incorporated into in the experimental glass ionomers sealant (Arg- TiO_2 (IP) GIC) which was employed in the current investigation for enhancing sealing ability [30, 45]. This was in line with a prior study that found that adding titanium oxide (TiO_2) nanoparticles to GIC improves enamel surface bonding compared to using regular glass ionomers cements [30]. As for the increase of the microleakage percentage in the (IP) GIC group, this may be attributed to the fact that the pre-treatment etching of the enamel surface produced rough texture and micro-tags thus trapped air bubbles that prevent flow of the sealant and increases microleakage [45]. However, some researchers found no appreciable difference in microleakage when teeth were mechanically prepared prior to applying a pit and fissure sealant versus non-mechanically treated with only phosphoric acid etching [46, 47].

A crucial factor that may have an impact on the sealant's retention is its penetration depth [48] which is consequently related to both the morphology of the fissures and the characteristics of the materials [49]. In the present study, the dye penetration technique was recommended because it is more precise when compared with other bacterial penetration methods in the oral cavity as the dye is more easily diffused than bacteria and their metabolic products [50]. Regarding the microscope depiction in Fig. 3, the experimental Arg- TiO_2 (IP) GIC group was found to be better for sealing ability as it showed significantly less dye penetration ability compared to the control (IP) GIC group. The wettability of the hydrophilic pit and fissure sealant on the enamel and the capillarity pressure control how deeply the sealant penetrates the enamel [34]. A previous study reported that GIC containing TiO_2 nano-particles seems to be more hydrophilic than conventional cement, and a wet surface helps its retention, this explains the good wettability and hence the less microleakage of the experimental Arg- TiO_2 (IP) GIC group [30]. However, the presence of dye penetration in this group may be due to the thermocycling procedure, as glass ionomer is affected by heat [51].

GIC chemically binds to enamel due to the interaction between carboxylate groups in polyacrylic acid and calcium ions in tooth tissue [52]. According to our findings, conventional (IP) GIC had enamel shear bond strengths that were lower than those of Arg- TiO_2 (IP) GIC. However, Alqarni and Elkweathey [45] demonstrated that a formation of

minerals or salts as a result of the reaction between acid and enamel hydroxyapatite might be a factor that prevent the intimate contact between sealant and enamel. Meanwhile, the previous finding could explain the extensive gap found throughout the sealant-enamel inter surfaces that appeared in the SEM images of the control (IP) GIC group at higher magnification.

Based on a previous study [52], dental substrate is one of the factors that affect the bond strength. In our study, enamel shear bond strength values increased in the experimental sealant. TiO_2 nanoparticles may reduce the number of glass particles on the surface of the (IP) GIC powder, which would cause a massive reaction between acid and nanoparticles thus sustaining the maximum ultimate load. According to SEM studies, some deposited microparticles were found within the matrix; these particles were revealed to be TiO_2 nanoparticle clusters that agglomerated because of their angular and semispherical morphology. These observations were made in response to the distinct properties observed in the IP GIC enhanced with TiO_2 nanoparticles. However, a microcrack within the salt matrix was found; the reason behind it is the weak ionic interaction that exists between the TiO_2 nanoparticles and the GIC particles [30]. On the other hand, an earlier work [29] demonstrated that adding TiO_2 nanoparticles to regular FX-II GIC powder results in the appropriate interaction of glass particles and nanoparticles. Furthermore, the results of the EDX data presented in our study have similar values as a study done using standard Fuji IX (GC). The results of the EDX study revealed greater TiO_2 concentrations, a lower carbon content, and greater oxygen concentrations.

According to the findings of our investigation, adding 1% Arg (w/w) to GIC didn't appear to have a negative impact on its mechanical properties. However, the present results for AFM images exhibited changes in surface textures and surface topography when the Arg- TiO_2 was added to (IP) GIC. It was demonstrated by Nadeem et al. [16] that, strong ionic bonds are created when the electronegative F ion and positively charged Arg guanidinium group come into touch, concentrating the forces in the specimen discs' core (mass) thus decrease the surface roughness at lower Arg concentrations (1% or 2%).

Findings in EDX analysis revealed that strontium was not detected in the experimental Arg- TiO_2 (IP) GIC though it was found in (IP) GIC. The addition of 3% TiO_2 nanoparticles and 1%Arg changed the elemental composition of (IP) GIC, but had no negative effect on the material's mechanical characteristics or surface roughness. Our findings may be explained by the fact that Arg substitutes the strontium ions which has a filler effect and thus has no negative impacts on the shear bond strength and surface roughness. However, experimental research revealed that the external addition of Arg filler at lower concentrations might not contribute to an even substitution of the elements but instead generated a calcium-fluoro-aluminum-silicate complex at the mass's center that was Arg-encapsulated [16]. On the other hand, when TiO_2 nanoparticles and Arg were added to (IP) GIC, the F concentration rose, likely as a result of the proper interaction between glass particles and TiO_2 nanoparticles without being impacted by the incorporation of Arg [29].

One of the most significant benefits of glass ionomer cements is fluoride release [53]. In our research, fluoride released from all specimens showed a pattern of initial rapid release in the first 12 h, followed by a marked decrease only for the glass ionomer Ionofil Plus (IP) until 24 h. The (IP) GIC group used as a control released lower values of fluoride amount (13.9 ppm) after 12 h than the Arg- TiO_2 (IP) GIC (17.7 ppm). Some authors evaluated Ionofil molar and reported close values (19.7 ppm) [54] and others reported greater values (32.80 ppm) than those found in our study [55]. Our findings could be explained by the effect of an initial 24-h burst release of F by GIC, followed by a marked decrease, which has been well documented in previous studies [56, 57].

Analysing the impact of nanotechnology on the mechanical characteristics of GICs has been the topic of several studies [30, 54]. In earlier studies, TiO_2 nanoparticles were added to glass ionomer cements to change some characteristics, such as fluoride release. According to Elsaka et al. [31], there were no appreciable changes in the fluoride release of glass ionomer cements reinforced with TiO_2 nanoparticles at various concentrations (3%, 5%, and 7%) after a 1-month evaluation. Our findings, however, are consistent with those of other authors who have added TiO_2 nanoparticles to glass ionomer cements and have found that the amount of fluoride released has increased [58]. Nevertheless, some authors demonstrated a potential interaction between Arg and F [59, 60]. A previous study reported that the release of fluoro-alumino-silicate glass (Al, Si, and F) in the Arg group was greater than their release in the control group [16]. Research has demonstrated a significant positive association between the ion release potential of GIC and the arginine-alumino-silicate-fluoride complex that was generated by the addition of Arg to GIC. In contrast, more ions are released at higher Arg concentrations, according to the theories of several authors [59, 60]. They stated that the ion release may be restricted by concentrated attractive interactions between fluoro-alumino-silicate glass and the low concentration of Arg. It is evident that the addition of 3% TiO_2 nanoparticles and 1% Arg (w/w) to GICs changed the material's chemical spatial configurations and improved F release without affecting its mechanical properties.

Demineralization may become more severe if bacteria colonize morphologically vulnerable sites, such as developing molar teeth. Preventing infection is crucial because bacteria can use fissures and pits in enamel to colonize [61]. It is well known that GIC may have an anti-caries action and has the capacity to release fluoride. GIC does have a stronger caries-inhibiting capacity than resin-composites because of its ability to produce F [62], however the F that is released has little effect on bacterial biofilms that are close to the restorations [14, 63, 64]. Therefore, in order to increase the antibacterial action of GIC against the microbes causing caries, various studies have attempted to include antimicrobial compounds [14, 64–67]. In the present study, we found that adherent *L. rhamnosus* bacterial count [25.9 ± 1.2] had the highest count from different adherent bacterial in Arg–TiO₂ (IP) GIC group as well as had higher count compared to other adherent *L. rhamnosus* bacterial count in the control group (without GIC) and (IP) GIC group. Moreover, we noticed the lack of adherent *S. mutans* bacterial count [12.7 ± 1.6] compared to planktonic/adherent *S. mutans* bacterial count in the control group and (IP) GIC group. According to Nadeem et al., Arg may slow the growth of arginolytic commensals bacteria [16]; in contrast, the released F may prevent the growth of planktonic *S. mutans*. The inclusion of a prebiotic biofilm modifier (Arg) in (IP) GIC favors probiotic bacteria (*L. rhamnosus*) over arginolytic commensals (*A. viscosus*) and competes with pathogenic *S. mutans* for adhesion and nutrition with/without F, this may also account for some of our findings [68–70]. Additionally, the rivalry of Arg metabolism among bacteria to biosynthesize amino acids for their growth is the reason why probiotic bacteria are more prevalent than harmful bacteria [71]. The Arg–TiO₂ GIC favored the growth of *L. rhamnosus*. This is because the inclusion of a prebiotic biofilm modifier (Arg) in GIC act as substrate for probiotic bacteria *L. rhamnosus* and allow them to compete with other bacteria (*S. mutans* and *Actinomyces viscosus*) on the adhesion site and nutrition thus probiotic bacteria *L. rhamnosus* increases its adherence and profile growth and its count on the Arg–TiO₂ GIC, while the other bacteria dislodged from the Arg–TiO₂ GIC surface and increase in the planktonic model.

On the other hand, the GIC control group didn't contain Arg so could not allow probiotic bacteria to adhere on its surface and compete with other bacteria so it increased in planktonic model. As there is no problem with antimicrobial resistance in pathogens, in contrast to the previously considered antibacterial agents, hence we adopted a biofilm modulation technique in the current study [72, 73]. The presence of a naturally occurring amino acid that has a prebiotic action helps to maintain or restore biofilm's equilibrium around the restoration by favorably promoting the growth of good bacteria in contrast to oral pathogens. Therefore, the action of the bacteria on the tooth and the interference of their by-product with the developing dental caries are more crucial than the type of bacteria present. Alternatively, Elsaka et al. [31] discovered comparable antibacterial activity outcomes for restorative GIC Kavitan Plus (SpofaDental) samples supplemented with 3%, 5%, and 7% (w/w) TiO₂ nanopowder when *S. mutans* (ATCC 27351) was in direct contact with them. However, it has been previously established that the generation of reactive oxygen species (ROS), specifically hydroxyl free radicals and peroxide, is how TiO₂ nanoparticles exert their antibacterial action [74].

The outcomes of this laboratory study suggested that adding TiO₂ nanoparticles and Arg to (IP) GIC would enhance its ability to prevent dental caries by modulating the biofilm to maintain microbial equilibrium. In addition, this supplementation improves the more constant fluoride release and the mechanical properties of the (IP) GIC material. Likewise, by creating a symbiotic biofilm, Arg–TiO₂ (IP) GIC will be able to prevent demineralization and maintain the health of dental surfaces. Hence, the above results from the theoretical level can be used to help choose a good treatment protocol for sealing pits and fissures for high caries-indexed patients.

5 Conclusion

Under the limitation of the following study, the incorporation of 3%TiO₂ nanoparticles and 1% L-arginine in (IP) GIC enhanced the mechanical properties with a more fluoride release and promising antimicrobial efficiency. More in vivo investigations for biocompatibility and physical–chemical properties are required in order to confirm the suitability of Arg–TiO₂ (IP) GIC for clinical use.

Acknowledgements Not applicable

Author contributions HE, EA and AY conceptualized the study. HE planned the experiments. EA and AY conducted the experiments and analysed the data. HE, EA, ES, and AY wrote the manuscript. All authors read the final manuscript and agreed to be accountable for all aspects of the work.

Funding Open access funding provided by The Science, Technology & Innovation Funding Authority (STDF) in cooperation with The Egyptian Knowledge Bank (EKB). This research did not receive any specific grant from funding agencies in the public, commercial, or not-for-profit sectors.

Data availability The datasets used and/or analysed during the current study are available from the corresponding author upon reasonable request.

Declarations

Ethics approval and consent to participate All performed procedures of this study were carried out in accordance with relevant ethical guidelines and regulations of the Helsinki Declaration. The Medical Research Ethics Committee (MREC), National Research Centre of Egypt (33 El Bohouth St., Dokki, Giza, Egypt) with reference number “24402/2023”, approved all experimental protocols. For the collection of isolated teeth and saliva collection from a single donor, informed consent was obtained from all participants.

Consent for publication Not applicable.

Competing interests The authors declare that they have no competing interests.

Open Access This article is licensed under a Creative Commons Attribution 4.0 International License, which permits use, sharing, adaptation, distribution and reproduction in any medium or format, as long as you give appropriate credit to the original author(s) and the source, provide a link to the Creative Commons licence, and indicate if changes were made. The images or other third party material in this article are included in the article's Creative Commons licence, unless indicated otherwise in a credit line to the material. If material is not included in the article's Creative Commons licence and your intended use is not permitted by statutory regulation or exceeds the permitted use, you will need to obtain permission directly from the copyright holder. To view a copy of this licence, visit <http://creativecommons.org/licenses/by/4.0/>.

References

1. Bromo F, Guida A, Santoro G, Peciarolo M, Eramo S. Pit and fissure sealants: review of literature and application technique. *Minerva Stomatol.* 2011;60:529–41.
2. Young DA, Nový BB, Zeller GG, Hale R, Hart TC, Truelove EL, et al. The American dental association caries classification system for clinical practice: a report of the American dental association council on scientific affairs. *J Am Dent Assoc.* 2015;146:79–86.
3. Naaman R, El-Housseiny AA, AlAmoudi N. The use of pit and fissure sealants—a literature review. *Dent J.* 2017;5:34.
4. Beauchamp J, Caulfield PW, Crall JJ, Donly KJ, Feigal R, Gooch B, et al. Evidence-based clinical recommendations for the use of pit-and-fissure sealants: a report of the American Dental Association Council on scientific affairs. *J Am Dent Assoc.* 2008;139:257–68.
5. Azarpazhooh A, Main PA. Pit and fissure sealants in the prevention of dental caries in children and adolescents: a systematic review. *J Can Dent Assoc.* 2008;74:171–8.
6. Mount GJ. *Color atlas of glass ionomer cement.* 2nd ed. London: Martin Dunitz; 2002.
7. Sidhu SK, Schmalz G. The biocompatibility of glass-ionomer materials: a status report for the American Journal of Dentistry. *Am J Dent.* 2001;14:387–96.
8. Wiegand A, Buchalla W, Attin T. Review on fluoride-releasing restorative materials—fluoride release and uptake characteristics, antibacterial activity and influence on caries formation. *Dent Mater.* 2007;23:343–62.
9. Forsten L. Fluoride release and uptake by glass-ionomers and related materials and its clinical effect. *Biomaterials.* 1998;19:503–8.
10. Nicholson JW. Adhesion of glass-ionomer cements to teeth: a review. *Int J Adhes Adhes.* 2016;69:33–8.
11. Yamakami SA, Ubaldini AL, Sato F, Medina Neto A, Pascotto RC, Baesso ML. Study of the chemical interaction between a high-viscosity glass ionomer cement and dentin. *J Appl Oral Sci.* 2018;26:e20170384.
12. Forss H, Widström E. Reasons for restorative therapy and the longevity of restorations in adults. *Acta Odontol Scand.* 2004;62:82–6.
13. Dang MH, Jung JE, Lee DW, Song KY, Jeon JG. Recovery of acid production in *Streptococcus mutans* biofilms after short-term fluoride treatment. *Caries Res.* 2016;50:363–71.
14. Wang SP, Ge Y, Zhou XD, Xu HHK, Weir MD, Zhang KK, et al. Effect of anti-biofilm glass-ionomer cement on *Streptococcus mutans* biofilms. *Int J Oral Sci.* 2016;8:76–83.
15. Wiegand A, Buchalla W, Attin T. Review on fluoride-releasing restorative materials—fluoride release and uptake characteristics, antibacterial activity and influence on caries formation. *Dent Mater.* 2007;23:343–62.
16. Bijle MN, Ekambaram M, Lo ECM, Yiu CKY. Antibacterial and mechanical properties of arginine-containing glass ionomer cements. *Dent Mater.* 2020;36(9):1226–40.
17. González-Cabezas C, Fernández CE. Recent advances in remineralization therapies for caries lesions. *Adv Dent Res.* 2018;29:55–9.
18. Yin W, Hu DY, Li X, Fan X, Zhang YP, Pretty IA, et al. The anti-caries efficacy of a dentifrice containing 1.5% arginine and 1450 ppm fluoride as sodium monofluorophosphate assessed using quantitative light-induced fluorescence (QLF). *J Dent.* 2013;41(Suppl 2):S22–8.
19. Yin W, Hu DY, Li X, Fan X, Zhang YP, Pretty IA, et al. A clinical investigation using quantitative light-induced fluorescence (QLF) of the anticaries efficacy of a dentifrice containing 1.5% arginine and 1450 ppm fluoride as sodium monofluorophosphate. *J Clin Dent.* 2013;24:A15–22.
20. Hajishengallis E, Parsaei Y, Klein MI, Koo H. Advances in the microbial etiology and pathogenesis of early childhood caries. *Mol Oral Microbiol.* 2016;32:1–11.
21. Burne RA, Marquis RE. Alkali production by oral bacteria and protection against dental caries. *FEMS Microbiol Lett.* 2000;193:1–6.

22. Zheng X, Cheng X, Wang L, Qiu W, Wang S, Zhou Y, et al. Combinatorial effects of arginine and fluoride on oral bacteria. *J Dent Res*. 2015;94:344–53.
23. Huang X, Zhang K, Deng M, Exterkate RAM, Liu C, Zhou X, et al. Effect of arginine on the growth and biofilm formation of oral bacteria. *Arch Oral Biol*. 2017;82:256–62.
24. Agnello M, Cen L, Tran NC, Shi W, McLean JS, He X. Arginine improves pH homeostasis via metabolism and microbiome modulation. *J Dent Res*. 2017;96:924–30.
25. Tada A, Nakayama-Imaohji H, Yamasaki H, Hasibul K, Yoneda S, Uchida K, et al. Cleansing effect of acidic L-arginine on human oral biofilm. *BMC Oral Health*. 2016;16:40.
26. Sharma S, Lavender S, Woo JR, Guo L, Shi W, Kilpatrick-Liverman LT, et al. Nanoscale characterization of effect of L-arginine on *Streptococcus mutans* biofilm adhesion by atomic force microscopy. *Microbiology*. 2014;160:1466–73.
27. Dhull KS, Nandlal B. Comparative evaluation of fluoride release from PGR-composites and compomer on application of topical fluoride: an in vitro study. *J Indian Soc Pedod Prevent Dent*. 2009;27:27–32.
28. Moshaverinia A, Ansari S, Moshaverinia M, Roohpour N, Darr JA, Rehman I. Effect of incorporation of hydroxyapatite and fluoroapatite nanobioceramics into conventional glass ionomer cements (GIC). *Acta Biomater*. 2008;4:432–40.
29. Wang L, D'Alpino PH, Lopes LG, Pereira JC. Mechanical properties of dental restorative material: relative contribution of laboratory test. *J Appl Oral Sci*. 2003;11:162–7.
30. Garcia-Contreras R, Scougall-Vilchis RJ, Contreras-Bulnes R, Sakagami H, Morales-Luckie RA, Nakajima H. Mechanical, antibacterial and bond strength properties of nano-titanium-enriched glass ionomer cement. *J Appl Oral Sci*. 2015;23(3):321–8.
31. Elsaka SE, Hamouda IM, Swain MV. Titanium dioxide nanoparticles addition to a conventional glass-ionomer restorative: influence on physical and antibacterial properties. *J Dent*. 2011;39:589–98.
32. Faul F, Erdfelder E, Lang AG, Buchner AG. *Power 3: a flexible statistical power analysis program for the social, behavioral, and biomedical sciences. *Behav Res Methods*. 2007;39(2):175–91. <https://doi.org/10.3758/bf03193146>.
33. Schwimmer Y, Beyth N, Ram D, Mijiritsky E, Davidovich E. Laser tooth preparation for pit and fissure sealing. *Int J Environ Res Public Health*. 2020;17:7813.
34. Khogli AE, Cauwels R, Vercruyse C, Verbeeck R, Martens L. Microleakage and penetration of a hydrophilic sealant and a conventional resin-based sealant as a function of preparation techniques: a laboratory study. *Int J Paediatr Dent*. 2013;23(1):13–22. <https://doi.org/10.1111/j.1365-263X.2011.01218.x>.
35. Arafa AM, Aboalazm E, Kamel MH. The effect of mechanical and chemo-mechanical temporary cement cleaning methods on shear bond strength with self-adhesive resin cement (an in-vitro study). *BMC Oral Health*. 2022;22(1):648. <https://doi.org/10.1186/s12903-022-02672-7>.
36. Barroso JM, Torres CP, Lessa FCR, Pécora JD, Palma-Dibb RG, Borsatto MC. Shear bond strength of pit-and-fissure sealants to saliva-contaminated and noncontaminated enamel. *J Dent Child*. 2005;72(3):95–9.
37. Teymoornezhad K, Alaghehmand H, Daryakenari G, Khafri S, Tabari M. Evaluating the microshear bond strength and microleakage of flowable composites containing zinc oxide nano-particles. *J Electron Physician*. 2016;8(11):3289.
38. Osorio E, Osorio R, Zantotto ED, Peitl O, Toledano-Osorio M, Toledano M. SEM and AFM characterization of surface of two RMGICs for degradation before and after modification with bioactive glass ceramic. *J Adhes Sci Technol*. 2016;30(6):621–32.
39. Elgamily H, Ghallab O, El-Sayed H, Nasr M. Antibacterial potency and fluoride release of a glass ionomer restorative material containing different concentrations of natural and chemical products: an in-vitro comparative study. *J Clin Exp Dent*. 2018;10(4):e312–20.
40. Rudney JD, Hickey KL, Ji Z. Cumulative correlations of lysozyme, lactoferrin, peroxidase, S-IgA, amylase, and total protein concentrations with adherence of oral viridans streptococci to microplates coated with human saliva. *J Dent Res*. 1999;78(3):759–68. <https://doi.org/10.1177/00220345990780030801>.
41. Razak FA, Rahim ZH. The anti-adherence effect of Piper betle and Psidium guajava extracts on the adhesion of early settlers in dental plaque to saliva-coated glass surfaces. *J Oral Sci*. 2003;45(4):201–6. <https://doi.org/10.2334/josnusd.45.201>.
42. Farid AB, Omar AZ. Natural products for dental caries prevention. *J Med Food*. 2004;7:381–3.
43. Topcuoglu N, Ozan F, Ozyurt M, Kulekci G. In vitro antibacterial effects of glass-ionomer cement containing ethanolic extract of propolis on *Streptococcus mutans*. *Eur J Dent*. 2012;6:428–35.
44. Marković D. Microleakage, adaptation ability and clinical efficacy of two fluoride releasing fissure sealants. *Vojnosanit Pregl*. 2012;69(4):320–5.
45. Alqarni M, Elkatehy W. Microleakage of different pit and fissure sealants. *Int J Dentistry Oral Sci*. 2017;4(10):532–6.
46. Feigal RJ. The use of pits and fissure sealants. *Pediatr Dent*. 2002;24:415–22.
47. Blackwood JA, Dilley DC, Roberts MW, Swift EJ Jr. Evaluation of pumice, fissure enameloplasty and air abrasion on sealant microleakage. *Pediatr Dent*. 2002;24:199–203.
48. Kakaboura A, Matthaiou L, Papagiannoulis L. In vitro study of penetration of flowable resin composite and compomer into occlusal fissures. *Eur J Paediatr Dent*. 2002;3:205–9.
49. Duangthip D, Lussi A. Effects of fissure cleaning methods, drying agents, and fissure morphology on microleakage and penetration ability. *Pediatr Dent*. 2003;25:527.
50. Jacobs MS, Windeler AS. An investigation of dental luting cement solubility as a function of the marginal gap. *J Prosthet Dent*. 1991;65(3):436–42.
51. Subramaniam P, Jayasurya S, Girish Babu KL. Evaluation of glass carbomer sealant and a moisture tolerant resin sealant—a comparative study. *Intl J Dental Sci Res*. 2015;39(5):429–34.
52. Magni E, Ferrari M, Hickel R, Ilie N. Evaluation of the mechanical properties of dental adhesives and glass-ionomer cements. *Clin Oral Investig*. 2010;14:79–87.
53. Salmerón-Valdés E, Scougall-Vilchis R, Alanis-Tavira J, et al. Comparative study of fluoride released and recharged from conventional pit and fissure sealants versus surface prereacted glass ionomer technology. *J Conserv Dent*. 2016;19:41.
54. Morales-Valenzuela AA, Scougall-Vilchis RJ, Lara-Carrillo E, Garcia-Contreras R, Hegazy-Hassan W, Toral-Rizo VH, Salmerón-Valdés EN. Enhancement of fluoride release in glass ionomer cements modified with titanium dioxide nanoparticles. *Medicine*. 2022;101:44.

55. Shiozawa M, Takahashi H, Iwasaki N. Fluoride release and mechanical properties after 1-year water storage of recent restorative glass ionomer cements. *Clin Oral Investig*. 2014;18:1053–60.
56. Salmerón-Valdés E, Scougall-Vilchis R, Alanis-Tavira J, et al. Comparative study of fluoride released and recharged from conventional pit and fissure sealants versus surface prereacted glass ionomer technology. *J Conserv Dent*. 2016;19:41.
57. Asmussen E, Peutzfeldt A. Long-term fluoride release from a glass ionomer cement, a compomer, and from experimental resin composites. *Acta Odontol Scand*. 2002;60(2):93–7.
58. Cibim DD, Saito MT, Giovani PA, et al. Novel nanotechnology of TiO₂ improves physical–chemical and biological properties of glass ionomer cement. *Int J Biomater*. 2017;17:1–11.
59. Heyda J, Hrobárik T, Jungwirth P. Ion-specific interactions between halides and basic amino acids in water. *J PhysChem*. 2009;113:1969–75.
60. Schneider CP, Shukla D, Trout BL. Arginine and the Hofmeister series: the role of Ion–Ion interactions in protein aggregation suppression. *J Phys Chem B*. 2011;115:7447–58.
61. Scribante A, Poggio C, Gallo S, Riva P, Cuocci A, Carbone M, et al. In vitro re-hardening of bleached enamel using mineralizing pastes: toward preventing bacterial colonization. *Materials*. 2020;13:818.
62. Krämer N, Schmidt M, Lücker S, Domann E, Frankenberger R. Glass ionomer cement inhibits secondary caries in an in vitro biofilm model. *Clin Oral Investig*. 2018;22:1019–31.
63. Dang MH, Jung JE, Lee DW, Song KY, Jeon JG. Recovery of acid production in *Streptococcus mutans* biofilms after short-term fluoride treatment. *Caries Res*. 2016;50:363–71.
64. Wiegand A, Buchalla W, Attin T. Review on fluoride-releasing restorative materials—fluoride release and uptake characteristics, antibacterial activity and influence on caries formation. *Dent Mater*. 2007;23(3):343–62.
65. Xie D, Weng Y, Guo X, Zhao J, Gregory RL, Zheng C. Preparation and evaluation of a novel glass-ionomer cement with antibacterial functions. *Dent Mater*. 2011;27:487–96.
66. Weng Y, Guo X, Gregory R, Xie D. A novel antibacterial dental glass-ionomer cement. *Eur J Oral Sci*. 2010;118:531–4.
67. Weng Y, Howard L, Chong VJ, Sun J, Gregory RL, Xie D. A novel furanone-modified antibacterial dental glass ionomer cement. *Acta Biomater*. 2012;8:3153–60.
68. Zheng X, Cheng X, Wang L, Qiu W, Wang S, Zhou Y, et al. Combinatorial effects of arginine and fluoride on oral bacteria. *J Dent Res*. 2015;94:344–53.
69. Huang X, Exterkate RA, Ten Cate JM. Factors associated with alkali production from arginine in dental biofilms. *J Dent Res*. 2012;91:1130–4.
70. He J, Hwang G, Liu Y, Gao L, Kilpatrick-Liverman LT, Santarpi P, et al. L-arginine modifies the exopolysaccharide matrix and thwarts *Streptococcus mutans* outgrowth within mixed-species oral biofilms. *J Bacteriol*. 2016;198:2651–61.
71. Price MN, Zane GM, Kuehl JV, Melnyk RA, Wall JD, Deutschbauer AM, et al. Filling gaps in bacterial amino acid biosynthesis pathways with high-throughput genetics. *PLoS Genet*. 2018;14:1–23.
72. Vasudevan R. Biofilms: microbial cities of scientific significance. *J Microbiol Exp*. 2014;1:84–98.
73. Gupta P, Sarkar S, Das B, Bhattacharjee S, Tribedi P. Biofilm, pathogenesis and prevention—a journey to break the wall: a review. *Arch Microbiol*. 2016;198:1–15.
74. Wang H, Tang B, Li X, Ma Y. Antibacterial properties and corrosion resistance of nitrogen-doped TiO₂ coatings on stainless steel. *J Mat Sci Technol*. 2011;27:309–16.

Publisher's Note Springer Nature remains neutral with regard to jurisdictional claims in published maps and institutional affiliations.